Supporting Information for

From molecular copper complexes to composite electrocatalytic materials for selective reduction of CO_2 to formic acid

Dr T. N. Huan, Dr. E. S. Andreiadis, Dr. V. Artero*
Laboratoire de Chimie et Biologie des Métaux
Univ. Grenoble Alpes, CNRS UMR 5249, CEA
17 rue des martyrs
38054 Grenoble cedex 9
vincent.artero@cea.fr

Dr. E. S. Andreiadis, Dr. P. Simon, Prof. M. Fontecave*
Laboratoire de Chimie des Processus Biologiques
Collège de France, Université Pierre et Marie Curie, CNRS UMR 8229,
11 place Marcelin Berthelot
75005 Paris
marc.fontecave@college-de-france.fr

Dr. E. Derat
Sorbonne Universités
UPMC Univ. Paris 06, UMR 8232
Institut Parisien de Chimie Moléculaire
75005 Paris, France

Dr. S. Cobo; Prof. G. Royal
Université Joseph Fourier Grenoble 1
Département de Chimie Moléculaire, UMR CNRS-5250
Institut de Chimie Moléculaire de Grenoble, FR CNRS-2607
BP 53, 38041 Grenoble Cedex 9,
France

Arno Bergmann, Prof. Peter Strasser
The Electrochemical Energy, Catalysis and Materials Science Laboratory
Department of Chemistry, Chemical Engineering Division,
Technical University Berlin
Straße des 17. Juni 124, 10623 Berlin, Germany

Jonathan Heidkamp; Prof. Holger Dau
Fachbereich Physik,

Freie Universität Berlin,
Arnimallee 14, D-14195 Berlin, Germany

Experimental Section

Chemicals

All chemicals including cyclam (98%), tetrabutylammonium tetrafluoroborate (n-Bu_4BF_4) (99%), $Cu(ClO_4)_2.6H_2O$ (99.9%), lactic acid (85% in water), DMF (99.8%) and MeCN (99.9%) were purchased from Sigma-Aldrich. Fluorine-doped tin oxide (FTO) coated glass slides with 7Ω/sq surface resistivity and a thickness of 600 nm were purchased from Solems (France). They were rinsed with acetone and deionized water in a sonication bath prior to use. Cu_2O was deposited on FTO electrodes by electrodeposition from 0.2M $CuSO_4.5H_2O$ and 3M lactic acid in 0.5M pH 12 K_2HPO_4/K_3PO_4 aqueous buffer at a constant potential of –0,3V vs Ag/AgCl for 1h (charge passed = 1.2 $C.cm^{-2}$).[1] Metallic copper was deposited on FTO electrodes through electrolysis of $Cu(NO_3)_2.3H_2O$ (0.05M) in aqueous KNO_3 (0.1 M) pH 6 at –0.1 V vs Ag/AgCl.[2] Electropolishing of polycrystalline copper plates was achieved in H_3PO_4 85% at 0.2V vs $Hg/HgSO_4$ for 15 minutes as previously described.[3]

Methods

SEM images and EDX spectra were recorded with a FEG-SEM (Leo 1530) operating at 5 kV and equipped with a Princeton Gamma-Tech EDX system operating at 15 kV. X-ray photoemission spectroscopy (XPS) analyses were performed with a Kratos Axis Ultra DLD using a high-resolution monochromatic Al-Kα line X-ray source at 1486.6 eV. Fixed analyzer pass energy of 20 eV was used for core level scans. Survey spectra were captured at pass energy of 160 eV. The photoelectron take-off angle was normal to the surface, which provided an integrated sampling depth of approximately 15 nm. All spectra were referenced with an external gold substrate with a binding energy of 84.0 eV for Au 4f. Data were analysed using the

XPSPEAK4.1 software; AFM measurements were done with a Bruker ICOM microscope. X-ray diffraction measurements have been performed with a Bruker D8 Advance equipped with a Goebel mirror and 2.5° soller as primary optic and 0.23° secondary soller and a scintillation counter as detector. Diffraction pattern were recorded between 25 and 80° at an incident angle of 1° with a step size of 0.06°. Cu-based reflections have been fitted with pseudo-Voigt profiles and the given crystallite sizes were estimated via Scherrer equation from the FWHM of the reflections which were corrected for instrumental broadening.

XAS measurements at the copper *K*-edge were performed at beamline KMC-1 of the Helmholtz-Zentrum Berlin for Materials and Energy (formerly BESSY II).[4] Spectra were collected at 20 K in absorption and fluorescence mode as described elsewhere.[5] The scan range of the excitation energy was 8843-10008 eV. The energy windows of the single channel analyzers for the 13 elements of the fluorescence detector were set to the K_α-emission of Cu. No filter foil was put between sample and detector. For energy calibration, the energy axis of the experimental data was shifted by an offset such that the first maximum in the derivative of the reference signal (Cu foil, 5 μm thick) aligned with the value of 8979 eV reported by Bearden and Burr.[6] The EXAFS oscillations were extracted by minimizing a "knot-spline" with 5 knots between 8999 and 10008 eV, which then was subtracted from the data. For Fourier transformation of the k3-weighted EXAFS oscillations, a cosine window function covering the first 10% and the last 40% of the data k range (2−16 Å−1) was used to suppress sideloop artifacts.

Electrochemical measurements were performed in a three electrode two-compartment cell using a Bio-logic SP300 potentiostat. FTO-coated glass electrodes (see inset in Figure 1, electrolytic tape was used to define a 1cm^2 electrode surface), rinsed with acetone and deionized water prior to use, were used as working electrodes throughout the study. Connection of the FTO electrode to the potentiostat was made via an alligator clip. Ag/AgCl/3M KCl (hereafter abbreviated as Ag/AgCl) was used as the reference electrode and placed in the same compartment as the working electrode. A platinum counter electrode was placed in a separate compartment connected by a glass-frit and filled with the electrolytic solution. All potential values are given versus the potential of the Fc^+/Fc couple added as an internal standard to the solution after the measurements.

Hydrogen evolution was analyzed with a Perkin-Elmer Clarus 500 gas chromatography equipped with a porapack Q 80/100 column (6' 1/8") thermostated at 40°C and a TCD detector thermostated at 100 °C. Carbon monoxide, methane and other volatile hydrocarbons from the gas phase were analyzed using a gas chromatograph (Shimadzu GC-2010) equipped with a methanizer, a flame induction detector (FID) and a shincarbon ST (Restek) column. Methanol was assayed by gaz chromatography (Shimadzu GC 2010) using an Rtx-1 column (Restek) and a flame induction detector (FID). Formate, oxalate and glyoxylate concentrations were determined by ionic exchange chromatography (883 Basic IC, Metrohm). Formaldehyde was analyzed using NASH and chromotropic acid methods.[7, 8] For cyclam, triazacyclononane and terpyridine detection, the Cu-based modified electrodes were washed several times with the same solution of aqueous hydrochloric acid (100 µL of 6M HCl). The solutions were collected together, neutralized by adding 4.9 ml of 60 mM of Na_2CO_3. After evaporation to dryness, 500µL of water and an excess (1 mg) of $CuCl_2.2H_2O$ were added. After 10 min, the suspension was centrifuged and the supernatant was analysed by reverse phase HPLC. Cyclam and terpyridine complexes were analysed on an Xbridge C18 column (Waters) with a water/acetonitrile 0.1% TFA gradient system. Triazacyclononane complex was analyzed on an Atlantis C18 column (Waters) with 0.1 M carbonate–bicarbonate buffer (pH 9.2). Detection was achieved by UV absorbance at 260 nm using a calibration curve obtained from cyclam, triazacyclononane and terpyridine solutions similarly treated. The collected fractions were finally analyzed by ESI mass spectrometry. Copper was quantified using an *in-situ* stripping electroanalytical method.[9] For the analysis, a glassy carbon electrode was used and first polished using alumina slurries (0.05 µm) in water and then ultrasonicated for 15 min in deinonized water. The Cu-based film was dissolved using 100µL of 6M aqueous hydrochloric acid and the resulting solution was added to a solution of 20 mM $Hg(OAc)_2$ (10 mL) in 0.1 M acetate buffer pH 5.2. Then, Hg and Cu were co-deposited from this solution on the glassy carbon electrode poised at –0.4V vs Ag/AgCl for 10 minutes. Different pulse voltammetry (DPV) was used to acquire the signal of Cu (I_1) over a potential scan range from –0.4 to 0.5V vs Ag/AgCl. The concentration of Cu was then determined with the formula given below thanks to a second measure achieved after addition of a standard 10 mM Cu^{2+} solution (200 µL) to the analyzed solution, and using DPV method to acquire the signal of Cu (I_2).

$$I_1 / I_2 = [Cu^{2+}]_{sample} / ([Cu^{2+}]_{sample} + [Cu^{2+}]_{added})$$

Quantification of formate within the film has been carried out using ionic exchange chromatography (see above) after Cu-based film was dissolved using 100µL of 6M aqueous hydrochloric acid. For carbonate/bicarbonate quantification, the dissolution step was carried out in a gas-tight vial and the headspace was analyzed for the presence of CO_2 using gas chromatography under similar conditions as for H_2 detection.

Electroactive surface area of the electrodes were determined under linear sweep voltammetric conditions using the Randles-Sevcik relationship for the one-electron reduction of $K_3[Fe(CN)_6]$ in phosphate buffer (pH = 7).[9, 10]

$$i_p = 2.69\times10^5 n^{3/2} D^{1/2} A C \nu^{1/2}$$

with i_p the peak current corresponding to the reduction of the redox species (Fe^{3+}/Fe^{2+} couple), n the number of transferred electrons (here n=1) , D the diffusion coefficient of $[Fe(CN)_6]^{3-}$ (6.2×10^{-6} $cm^2.s^{-1}$), A the electroactive surface area, C the molar concentration of $[Fe(CN)_6]^{3-}$ (2.5×10^{-3} M) and ν the scan rate (here 0.1 $V.s^{-1}$). Calculated values are provided in the caption of Figure S5.

Determination of the standard potential of the CO_2/HCOOH couple in DMF

Most of the method used below is directly taken from reference [11] but we reproduce it in full for the sake of clarity. Of note however is the fact that we do not include the interliquid junction potential in the value of the standard potential of the CO_2/HCOOH couple versus NHE but in a second stage when we refer it to the reference system used to measure electrochemical potentials.

We will first determine the standard potential of the CO_2/HCOOH couple in a solvent S and in the presence of a weak acid AH referred to the aqueous normal hydrogen electrode (NHE). The redox half-reaction reads as follows:

$$CO_{2(s)} + 2\ HA_{(s)} + 2\ e^- = HCOOH_{(s)} + 2A^-_{(s)}$$

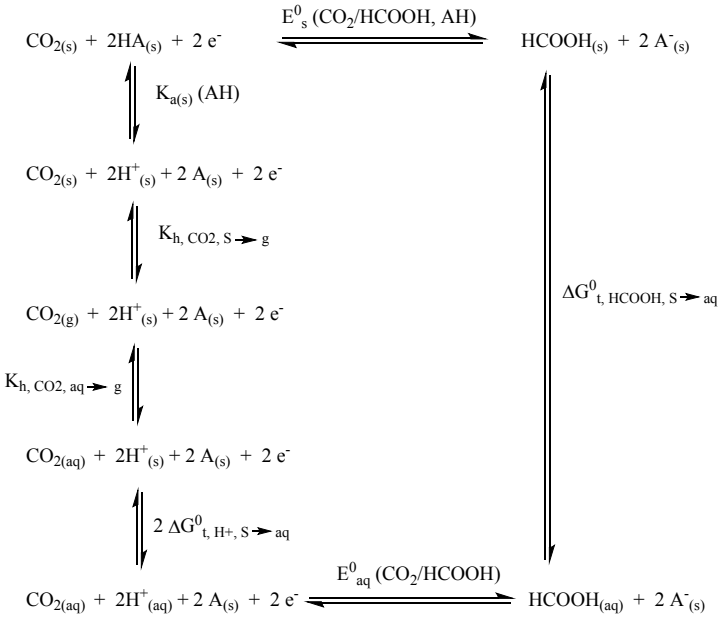

Scheme S1

We used the thermodynamic cycle shown in Scheme S1 and derived the following equation

$$E^0_S(CO_2/HCOOH,AH) = E^0_{aq}(CO_2/HCOOH) - \frac{RT ln 10}{F} pKa_{(S)}(AH) - \frac{RT}{2F} \ln\left(\frac{K_{h,\,CO_2,\,aq\rightarrow g}}{K_{h,\,CO_2,\,S\rightarrow g}}\right) - \frac{2\,\Delta G^0_{t,\,H^+,\,S\rightarrow aq} - \Delta G^0_{t,\,HCOOH,\,S\rightarrow aq}}{2F}$$

with

$E^0_{aq}(CO_2/HCOOH) = -0.11$ V vs NHE at pH 0 [12]

$\Delta G^0_{t,\,H^+,\,DMF\rightarrow aq} = 0.186\ eV$ [11, 13]

$\Delta G^0_{t,\,HCOOH,\,DMF\rightarrow aq} = -0.05\ eV$ (see below)

$K_{h,\,CO_2,\,S\rightarrow g} = \dfrac{P_{CO_2}/P^0}{[CO_2]_{(S)}/C^0}$, with $[CO_2]_{(S)}$ the solubility if CO_2 in the solvent of interest under $P_{CO2} = 10^5$ Pa; $P^0 = 10^5$ Pa and $C^0 = 1$ mol.L^{-1}

$[CO_2]_{DMF}$ = 0.2 mol.L^{-1} [14] and $[CO_2]_{aq}$= 0.038 mol.L^{-1} [15]

We obtain $E^0_{DMF}(CO_2/HCOOH, AH) = -0.342$ V vs NHE $- \frac{RTln10}{F} pKa_{(S)}(AH)$

Considering now that H_2CO_3 formed by hydration of CO_2 is the strongest acid in the CO_2-saturated DMF/H_2O (97:3 v/v) and using the pKa value of 7.37 previously determined for this couple in DMF,

We finally obtain**:**

$E^0_{DMF}(CO_2/HCOOH, H_2CO_3) = -0.78$ V vs NHE

To refer this potential versus the Fc^+/Fc couple, we used the experimentally determined value of $E(Fc^+/Fc) = 0.50$ V vs Ag/AgCl/KCl 3 mol.L^{-1} ($E_{Ag/AgCl}$ = 0.210 V vs NHE) and corrected it with the interliquid potential (0.142 V)[11] between the aqueous electrolyte of the Ag/AgCl electrode and the DMF solution containing n-Bu_4BF_4 (0.1 mol.L^{-1}). This yields $E_{DMF}(Fc^+/Fc)$ = 0.57 V vs NHE.

Thus **$E^0_{DMF}(CO_2/HCOOH, H_2CO_3) = -1.35$ V vs Fc^+/Fc**

Determination of the solvation free enthalpy variation for HCOOH for the transfer from DMF to water.

For the calculation of solvation free enthalpy, we used the SMD implicit solvation method[16] with the M05-2X DFT functional[17] and the TZVP basis.[18] We first check this method for the determination of the solvation energy of formate in water, for which a value of –74.6 kcal.mol^{-1} has been reported.[19, 20] We calculated a value of –73.39 kcal.mol^{-1}, close to the experimental value. We thus anticipate that this method could be quite accurate for the determination of solvation free enthalpy variations, since systematic errors will be compensated during the calculation.

The same method was then used for the calculation of the solvation free energy of formic acid in different solvants:

ΔG^0_{solv}(HCOOH, water) = –7.19 kcal.mol^{-1}
ΔG^0_{solv}(HCOOH, DMF) = –6.01 kcal.mol^{-1}
ΔG^0_{solv}(HCOOH, CH_3CN) = –5.74 kcal.mol^{-1}

thus,

$$\Delta G_{t,\ HCOOH,\ DMF\rightarrow aq}^{0} = -1.18\ kcal.mol^{-1} = -0.05\ eV$$

Supporting Figures

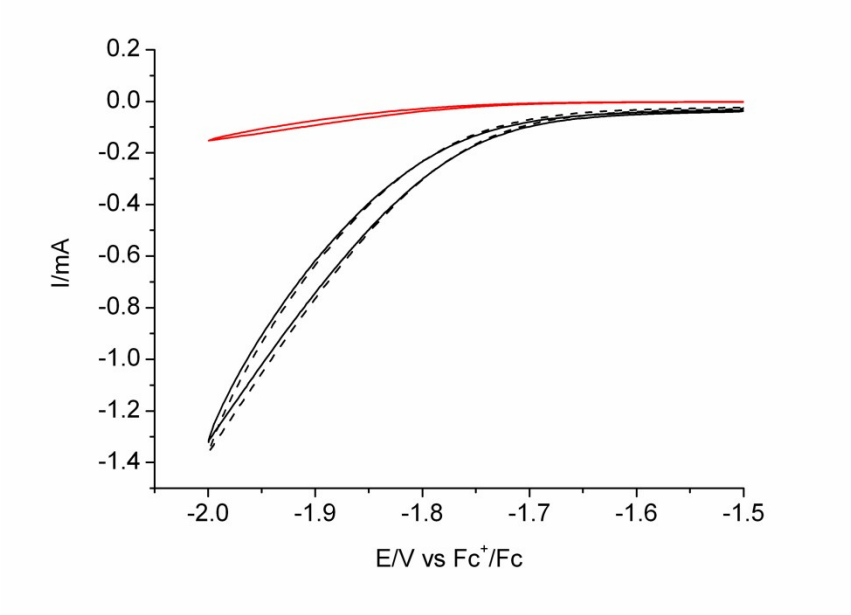

Figure S1. Cyclic voltammograms of the blue material deposited from $[Cu(cyclam)]^{2+}$ as described in Figure 1 successively measured in CO_2-saturated DMF solution (3% H_2O, 0.1M n-Bu_4NBF_4) (black, solid trace), after N_2 purge (red trace) and resaturation with CO_2 (black dashed trace).

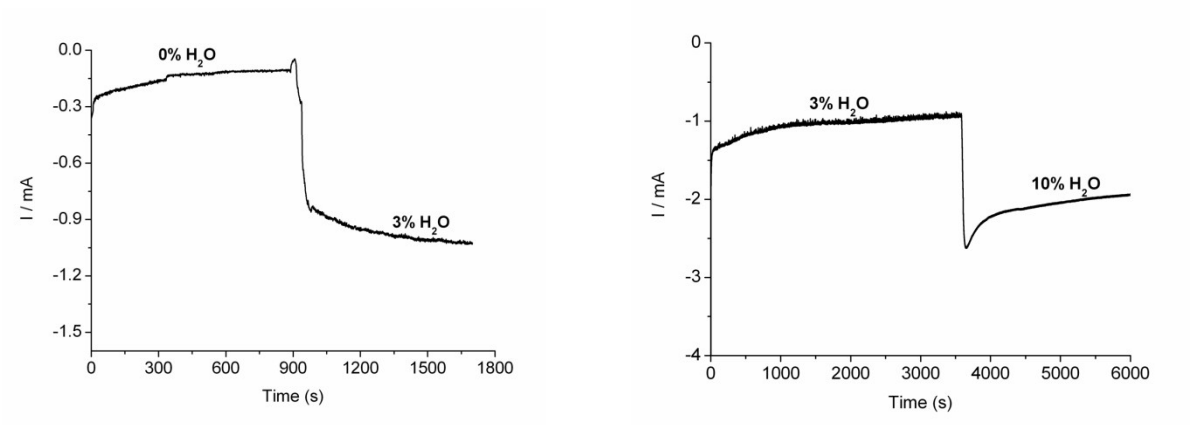

Figure S2: Effect of water concentration in DMF on current densities during electrolysis of CO_2-saturated solutions at -2.0 V vs Fc^+/Fc. A blue electrode material (a charge of 3C passed during electrodeposition from $[Cu(cyclam)]^{2+}$ was used. In the first experiment (left panel) the solvent

was pure DMF and water was added (3% final) after 900 s. In the second experiment (right panel), the solvent was DMF/H_2O (97:3 v/v) and water was added after 3500 s to reach 10%.

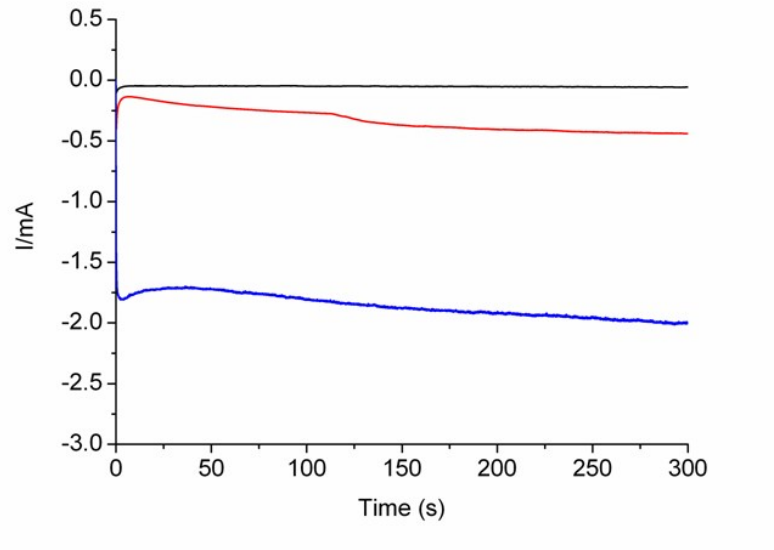

Figure S3. Evolution of the electrocatalytic current during potentiostatic deposition of the blue material from $[Cu(cyclam)]^{2+}$ at different potentials: –1.5 V vs Fc^+/Fc (black trace), –1.7 V vs Fc^+/Fc (red trace) and –2.0 V vs Fc^+/Fc (blue trace) on FTO electrodes (1cm^2) in CO_2-saturated DMF (3% H_2O, 1 M n-Bu_4NBF_4) solutions of $[Cu(cyclam)]^{2+}$ (1.3 mM, 6 mL).

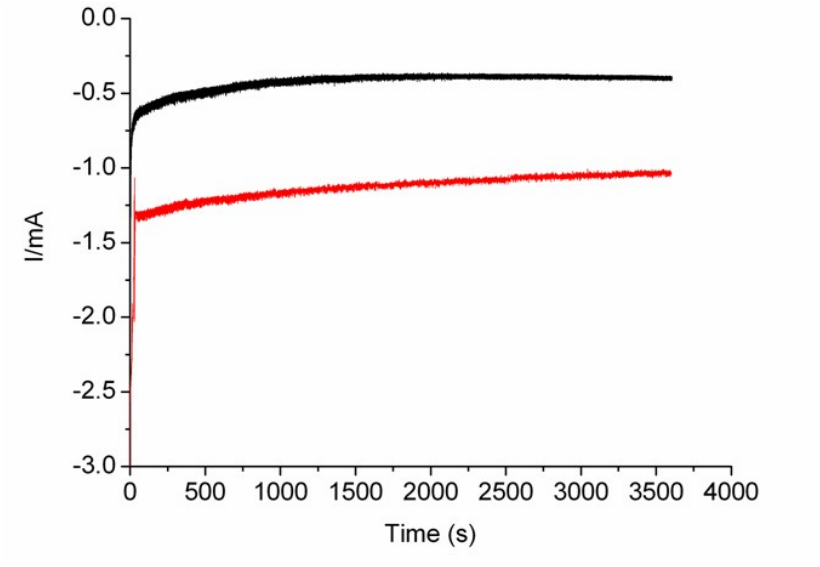

Figure S4. Evolution of the electrocatalytic current during potentiostatic deposition of the blue material at –2.0 V vs Fc^+/Fc on FTO electrodes (1 cm^2) in CO_2-saturated DMF (red trace) or CH_3CN (black trace) solutions of $[Cu(cyclam)]^{2+}$ (1.3 mM, 8 mL) added with 3% H_2O and 1 M n-Bu_4NBF_4.

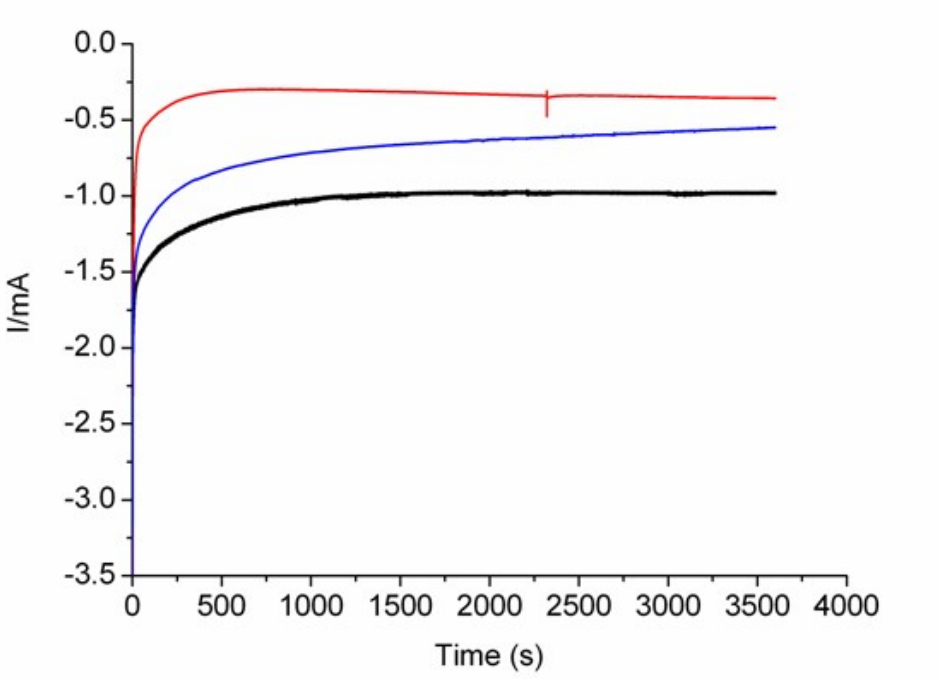

Figure S5. Evolution of the electrocatalytic current during potentiostatic CO_2 reduction assay at –2.0 v vs Fc^+/Fc in DMF/H_2O (3%) solution measured for blue materials (1cm^2_{geom}) obtained by electrodeposition from $[Cu(terpy)_2]^{2+}$ (red trace), $[Cu(TACN)]^{2+}$ (blue trace) and $[Cu(cyclam)]^{2+}$ (black trace). The faradic yields for formic acid production were found to be respectively 49, 68 and 86%.

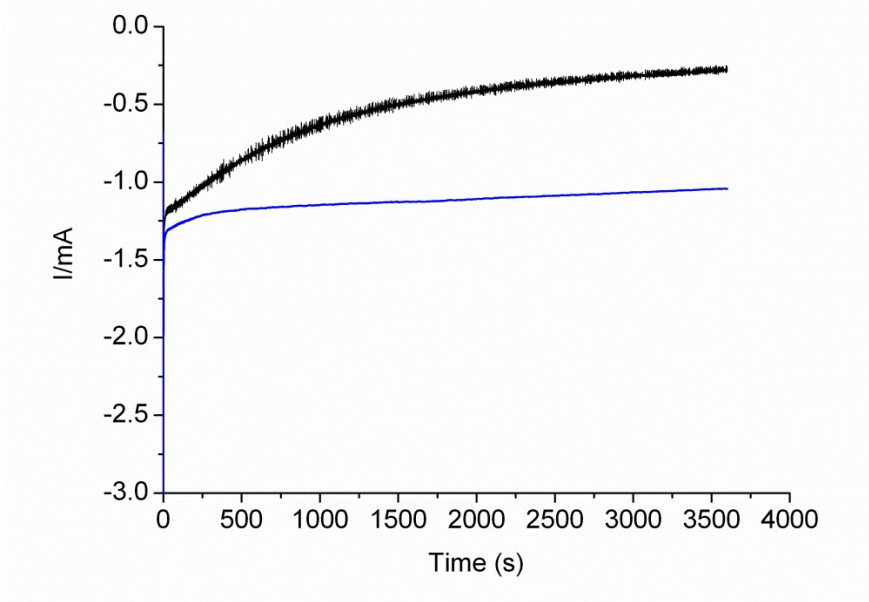

Figure S6. Evolution of the electrocatalytic current during potentiostatic CO_2 reduction assay at –2.0 v vs Fc^+/Fc in DMF/H_2O (3%) solution measured for the blue material obtained from $[Cu(cyclam)]^{2+}$ (blue trace, $1cm^2_{geom}$) and FTO electrode ($1cm^2_{geom}$) modified through electrodeposition as described for the preparation of the blue material but in the absence of cyclam ligand (black trace). The faradic yields for formic acid production was found to be 86-91% for the blue material and 58% for the material electrodeposited in the absence of the cyclam ligand.

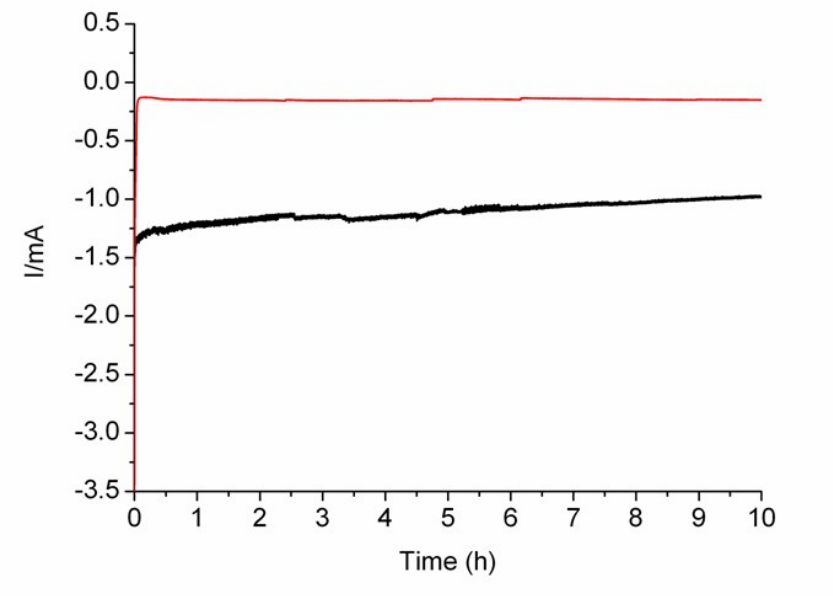

Figure S7. Long-term (10h) evolution of the electrocatalytic current during potentiostatic CO_2 reduction assay at –2.0 v vs Fc^+/Fc in DMF/H_2O (3%) solution measured on a blue material-modified FTO electrode (1cm^2, black trace, obtained from $[Cu(cyclam)]^{2+}$) and unmodified FTO electrode (red trace, 1 cm^2).

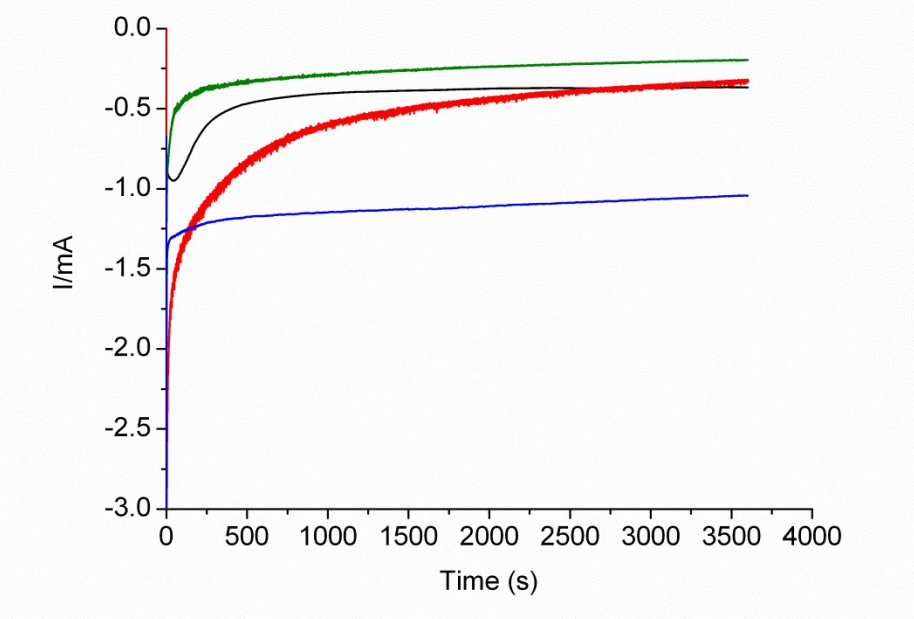

Figure S8. Evolution of the electrocatalytic current during potentiostatic CO_2 reduction assay at –2.0 v vs Fc^+/Fc in DMF/H_2O (3%) solution measured on various electrodes (geometrical area = 1cm^2; the measured electroactive surface area A is indicated for each electrode): blue material from $[Cu(cyclam)]^{2+}$ (blue trace, A = 2.26 cm^2), metallic copper electrodeposited on FTO (black trace, A = 2.55 cm^2), electro-polished polycrystalline Cu plate electrode (green trace, A = 1.32 cm^2) and Cu_2O electrodeposited on FTO (red trace, A = 2.08 cm^2) . The faradic yields for formic acid production was found to be 58% for electrodeposited metallic copper, 32% for electro-polished polycrystalline Cu plate electrode and 53% for the Cu_2O/FTO electrode. Under similar conditions, the blue material displays faradic yield of 88+/-3 %.

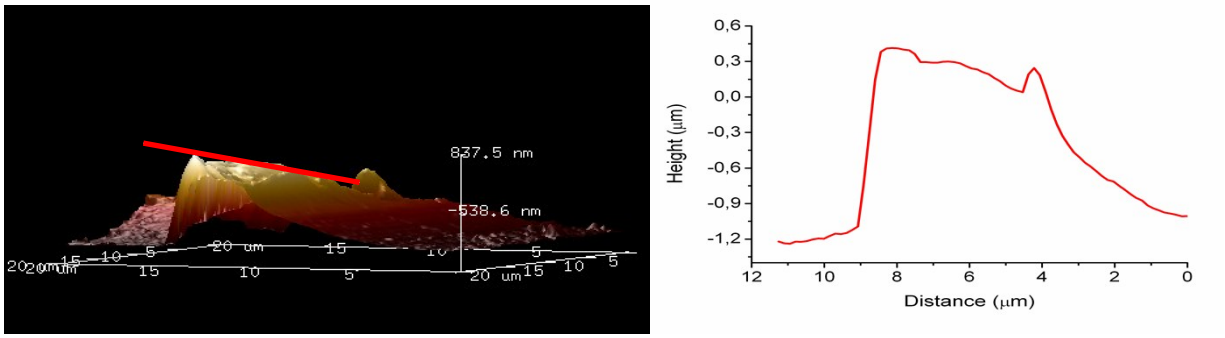

Figure S9: AFM image of the edge of a scratch made in the surface of a blue electrode material (left panel) and variations of the thickness of the film across the corresponding line mapping (right panel)

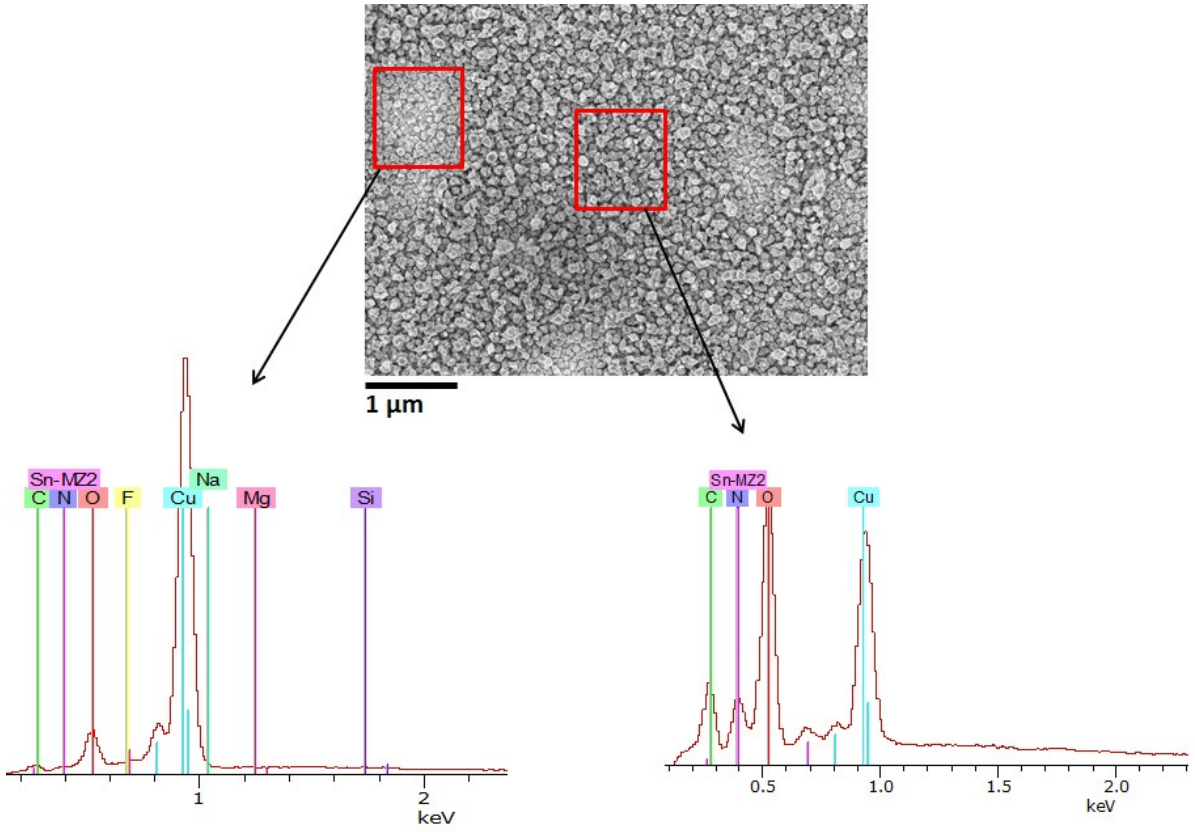

Figure S10. SEM image and Energy-dispersive X-ray spectroscopy (EDAX) spectrum of the blue material obtained from $[Cu(cyclam)]^{2+}$. Two differents areas are analyzed: on the left side, large particles (µm in diameter) and on the right side, nanoparticles with 100 nm diameter.

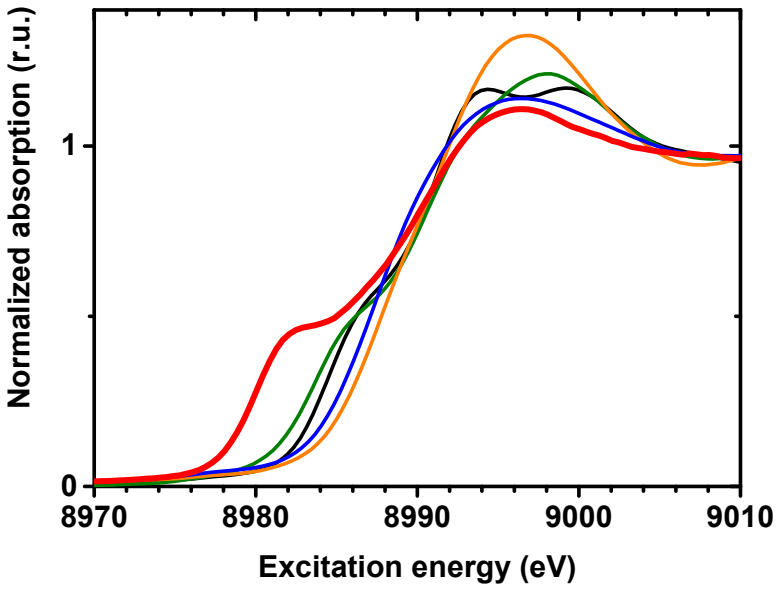

Figure S11. XANES spectra of Cu(II) compounds recorded at the Cu K edge: (**red**) blue material from $[Cu(cyclam)]^{2+}$ (deposition of $1C.cm^{-2}$), (**green**) Cu(II) oxide, (**orange**) Cu(II) oxalate, (**blue**) Cu(II) malachite and (**black**) $[Cu(cyclam)](ClO_4)_2$.

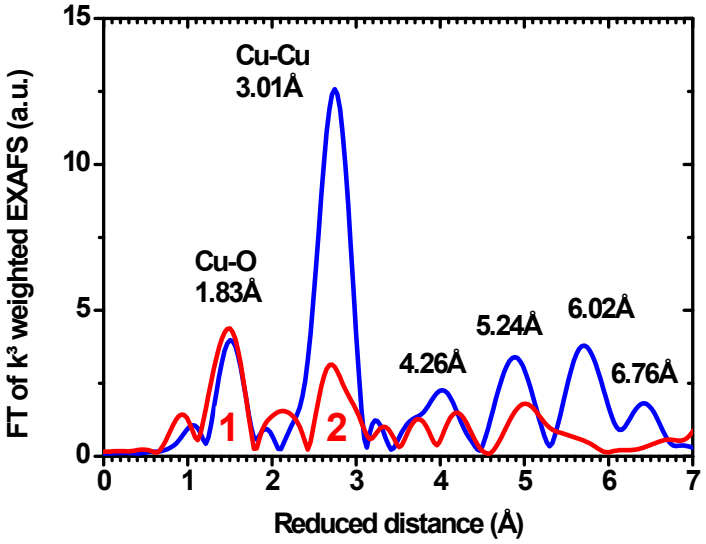

Figure S12. Fourier transforms of k^3-weighted EXAFS spectra recorded at the Cu K edge: (**red**) spectrum of the blue material from $[Cu(cyclam)]^{2+}$ (deposition of $1C.cm^{-2}$) after subtraction of metallic contribution and (**blue**) Cu(I) oxide (Cu_2O). The peaks of Cu(I) oxide are labeled with the absorber-ligand distances of the corresponding O and Cu coordination shells. The first and second main peaks in the Cu-based material spectrum are labeled with **1** and **2**. Peak **1** and **2** were fitted with a model based on the crystal structure of Cu(I) oxide. For peak **1**, the fitted Cu-O coordination yields a distance of R=1.86 ± 0.02 Å and, for peak **2**, the fitted Cu-Cu coordination a distance of R=2.98 ± 0.02 Å. These are a bit longer than the corresponding Cu(I) oxide distances and, therefore, indicate the presence of an additional Cu(II) species (see Table S1). This is supported by the fitted coordination number of N=2.4 ± 0.5 for peak **1** which is higher than N=2 for Cu-O in Cu(I) oxide and points towards Cu(II) species with N=4. The low amplitude of peak **2** indicates that the Cu(I) oxide in the blue material is very disordered at higher distances than 1.83Å.

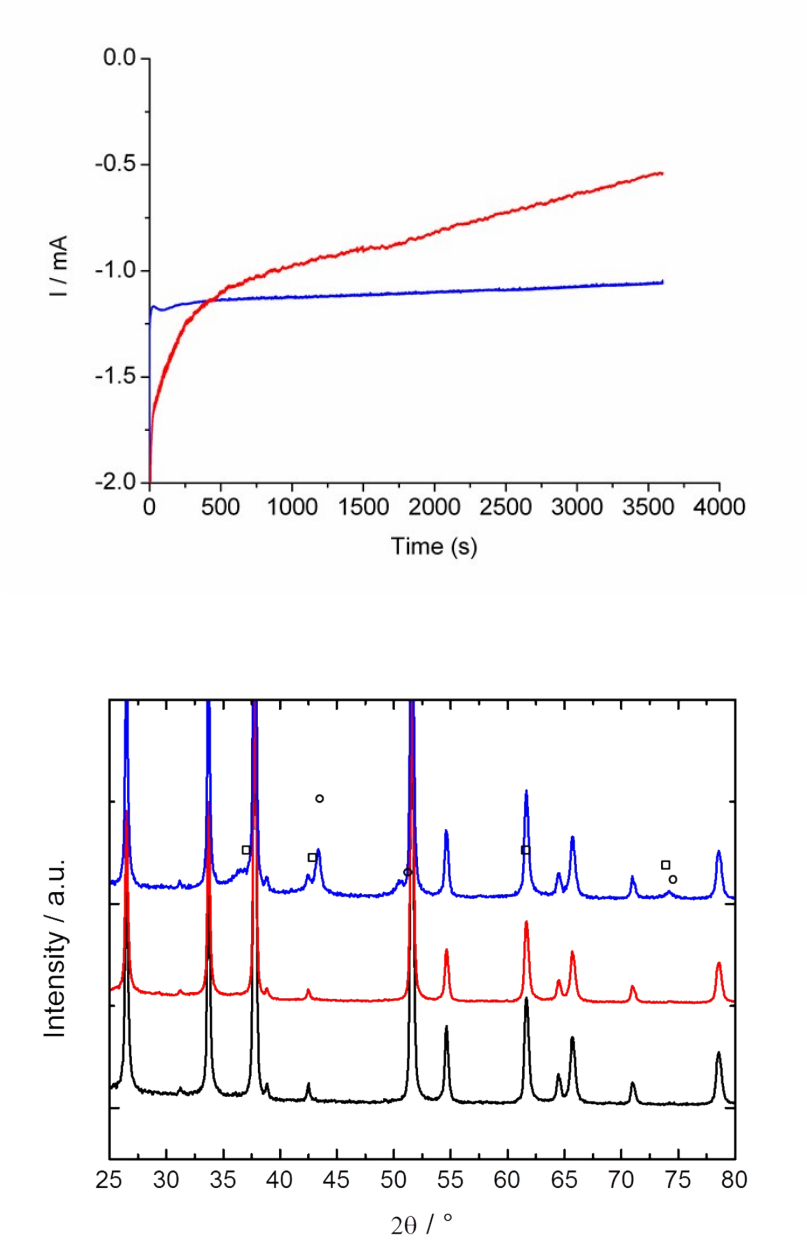

Figure S13. Top: Evolution of the electrocatalytic current during potentiostatic CO_2 reduction assay at –2.0 V vs Fc^+/Fc in DMF/H_2O (97:3 v/v) solution measured on FTO electrodes modified with the blue material (1cm^2) from $[Cu(cyclam)]^{2+}$. The electrodes differed by the quantity of charge passed during the deposition step: 1.0C (red trace) and 4.0C (blue trace); Bottom: XRD diffraction pattern recorded on the FTO substrates (black trace), 1C-deposited blue material film (red trace) and 4C-deposited blue material film (blue trace). Peaks assigned to Cu and Cu2O crystallites are labelled with circles and squares, respectively.

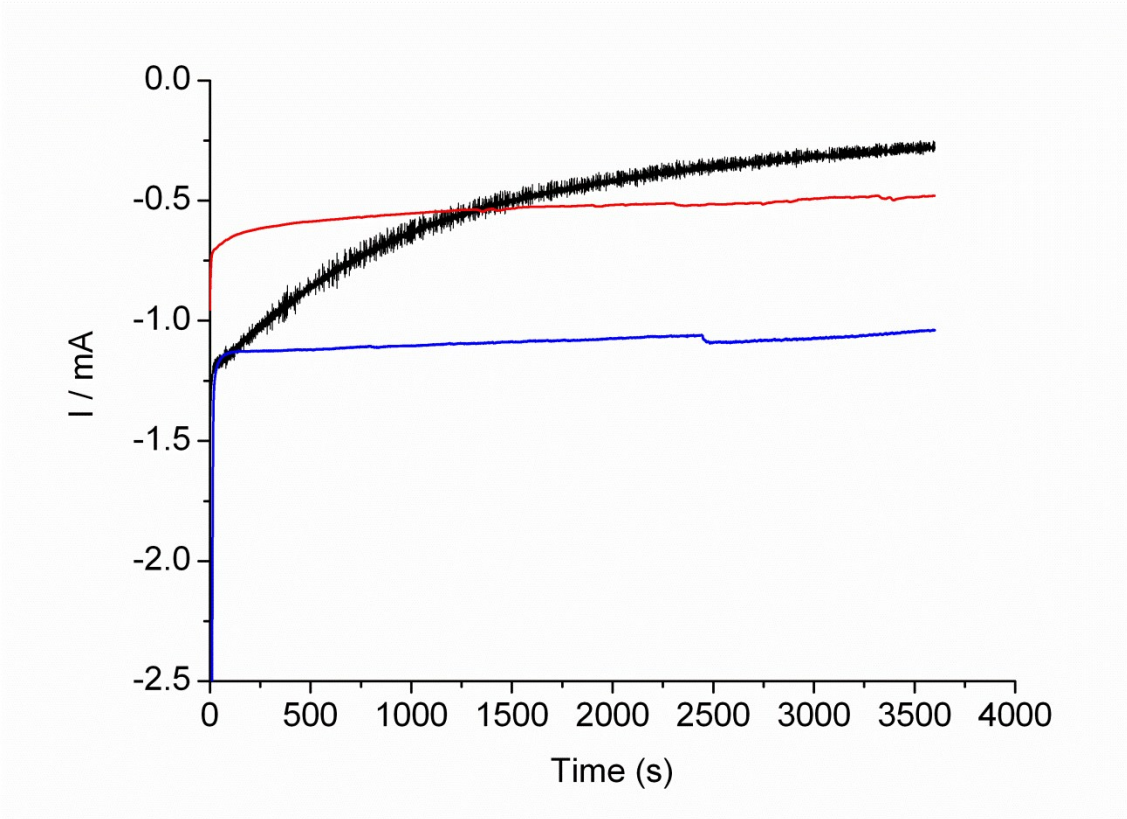

Figure S14. Evolution of the electrocatalytic current during potentiostatic CO_2 reduction assay at –2.0 V vs Fc^+/Fc in DMF/H_2O (3%) solution measured on FTO electrodes modified with the blue material (1cm^2) from $[Cu(cyclam)]^{2+}$ (4C passed the deposition) without O_2 plasma treatment (blue) and after 30 minutes O_2 plasma treatment at the power of 100W (red). Under these conditions, HPLC titration indicates almost complete removal of the cyclam ligand from the film. For comparison, the evolution of the electrocatalytic current under similar conditions but measured for the FTO electrode (1cm^2_{geom}) modified through electrodeposition as described for the preparation of the blue material but in the absence of cyclam ligand is shown as a black trace.

Compound	**First Cu-O/N distance [Å]**	**Coordination number N**
1C.cm^{-2} blue material from $[Cu(cyclam)]^{2+}$	1.86 ± 0.02	2.4 ± 0.5

Cu(I) oxide	1.83	2
Cu(II) malachite	1.93	2
Cu(II) oxalate	1.94	4
Cu(II) oxide	1.95	4
[Cu(cyclam)]$(ClO_4)_2$	2.03	4

Table S1. Selection of investigated Cu compounds ordered according to the respective Cu-O/N distance. The corresponding coordination numbers are presented in the third column. The Cu-O/N distances were determined by simulation of the EXAFS spectra of the compounds (curve fitting of k^3-weighted EXAFS spectra). For the blue material, the Cu-O distance and the coordination number were determined by simulation of the EXAFS spectrum as obtained after correction for a metallic contribution of 20%.

References

1. A. Paracchino, V. Laporte, K. Sivula, M. Gratzel and E. Thimsen, *Nat. Mater.*, 2011, **10**, 456-461.
2. W. Shang, X. Shi, X. Zhang, C. Ma and C. Wang, *Appl. Phys. A: Mater. Sci. Process.*, 2007, **87**, 129-135.
3. D. Y. Li, N. Li, G. F. Xia, Z. Zheng, J. L. Wang, N. Xiao, W. J. Zhai and G. Wu, *Int. J. Electrochem. Sci.*, 2013, **8**, 1041-1046.
4. F. Schaefers, M. Mertin and M. Gorgoi, *Rev. Sci. Instrum.*, 2007, **78**.
5. M. Risch, K. Klingan, J. Heidkamp, D. Ehrenberg, P. Chernev, I. Zaharieva and H. Dau, *Chem. Commun.* 2011, **47**, 11912-11914.
6. J. A. Bearden and A. F. Burr, *Reviews of Modern Physics*, 1967, **39**, 125-142.
7. S. B. Jones, C. M. Terry, T. E. Lister and D. C. Johnson, *Anal. Chem.*, 1999, **71**, 4030-4033.
8. W. M. Grant, *Anal. Chem.*, 1948, **3**, 267-269.
9. E. A. Mcgaw and G. M. Swain, *Anal. Chim. Acta*, 2006, **575**, 180-189.
10. A. J. Bard and L. R. Faulkner, *Electrochemical Methods, Fundamentals and Applications*, Wiley, New York, (2001). .
11. C. Costentin, S. Drouet, M. Robert and J. M. Saveant, *Science*, 2012, **338**, 90-94.
12. T. Reda, C. M. Plugge, N. J. Abram and J. Hirst, *Proc. Natl. Acad. Sci. USA*, 2008, **105**, 10654-10658.
13. Y. Marcus, *Ion Properties* p. 214.
14. A. Gennaro, A. A. Isse and E. Vianello, *J. Electroanal. Chem.*, 1990, **289**, 203-215.
15. D. R. Lide, P. R. Frederikse and Eds., *Handbook of Chemistry and Physics*, (CRC Press, Boca Raton, FL, ed 76, 1995).
16. A. V. Marenich, C. J. Cramer and D. G. Truhlar, *J. Phys. Chem. B*, 2009, **113**, 6378-6396.
17. Y. Zhao, N. E. Schultz and D. G. Truhlar, *J. Chem.Theory Comput.*, 2006, **2**, 364-382.
18. A. Schäfer, C. Huber and R. Ahlrichs, *J. Chem. Phys.*, 1994, **100**, 5829-5835.
19. Y. Marcus, *J. Chem. Soc. Faraday Trans.*, 1991, **87**, 2995-2999.
20. A. Bennaim and Y. Marcus, *J. Chem. Phys.*, 1984, **81**, 2016-2027.